Design, Fabrication and Optical Characterisation of Photonic Crystal based Quantum Cascade Lasers at Terahertz Frequencies

L. Andrea Dunbar, Virginie Moreau, Rolando Ferrini and Romuald Houdré

Laboratoire de physique des dispositifs semiconducteurs, Institut de photonique et d'électronique quantique, Faculté des sciences de base, École Polytechnique Fédérale de Lausanne, Lausanne CH-1015, Switzerland

andrea.dunbar@epfl.ch

Lorenzo Sirigu, Giacomo Scalari, Marcella Giovannini, Nicolas Hoyler and Jérôme Faist

Institute of Physics, University of Neuchâtel, 1 A.-L. Breguet, CH-2000 Switzerland

lorenzo.sirigu@unine.ch

Abstract: We designed, fabricated and characterised electrically injected quantum cascade lasers with photonic crystal reflectors emitting at terahertz frequencies (3.75 THz). These in-plane emitting structures display typical threshold current densities of 420 A/cm^2 and output powers of up to 2 mW under pulsed excitation. The emission characteristics are shown to be robust, as with increasing current the emission remains singlemode with no drift in wavelength, this results from the narrow reflectivity band of the photonic crystal reflectors.

OCIS codes: (130.3120) Integrated Optics, (130.0250) Optoelectronics (140.5960), Semiconductor Lasers, (230.5590) Quantum Well Devices.

References and links

1. J. Faist, F. Capasso, D. L. Sivco, C. Sirtori, A. L. Hutchinson, and A. Y. Cho, "Quantum Cascade Laser," *Science* **264,** 553–556 (1994).
2. M. Beck, D. Hofstetter, T. Aellen, J. Faist, U. Oesterle, M. Ilegems, E. Gini, and H. Melchior "Continuous Wave Operation of Mid-Infrared Semiconductor Laser at Room Temperature" *Science* **295,** 301–305 (2002).
3. S. John, "Strong localization of photons in certain disordered dielectric superlattices," Phys. Rev. Lett. **58,** 2486–2489 (1987).
4. E. Yablonovitch, "Inhibited Spontaneous Emission in Solid-state Physics and Electronics," Phys. Rev. Lett. **58,** 2059–2062 (1987).
5. K. Busch, S. Lölkes, R. B. Wehrspohn, and H. Föll *Photonic Crystals: Advances in Design, Fabrication and Characterization* (Wiley-VCH, Weinheim, 2004).
6. R. Colombelli, K. Srinivasan, M. Troccoli, O. Painter, C. F. Gmachl, D. M. Tennant, A. M. Sergent, D. L. Sivco, A. Y. Cho, and F. Capasso "Quantum Cascade Surface-Emitting Photonic Crystal Laser" *Science* **302,** 1374–1377 (2003).
7. M. Rochat, D. Hofstetter, M. Beck, and J. Faist "Long-wavelength ($\lambda \approx 16$ μm), room-temperature, single-frequency quantum-cascade lasers based on a bound-to-continuum transition" Appl. Phys. Lett. **79,** 4273–4271 (2001).
8. R. Köhler, A. Tredicucci, F. Beltram, H. E. Beere, E. H. Linfield, A. G. Davies, D. A. Richie, R. C. Lotti, and F. Rossi "Terahertz semiconductor-heterostructure laser"*Nature***417,** 156–159 (2002).

9. B. S. Williams, S. Kumar, Q. Hu, and J. L. Reno "Operation of terahertz quantum-cascade lasers at 164 K in pulsed mode and at 117 K in continuous-wave mode" Opt. Express **13,** 3331–3339 (2005).
10. R. Ferrini, D. Leuenberger, M. Mulot, M. Qiu, J. Moosburger, M. Kamp, A. Forchel, S. Anand, and R. Houdré "Optical Study of Two-Dimensional InP-Based Photonic Crystals by Internal Light Source Technique" IEEE J. Quantum Electron. **38,** 786–799 (2002).
11. E. Kuramochi, M. Notomi, S. Hughes, L. Ramunno, G. Kira, S. Mitsugi, A. Shinya, and T. Watanabe "Scattering Loss of Photonic Crystal Waveguides and Nanocavities induced by Structural Disorder" *CLEO Pacific Rim Tokyo Japan* **CTuE1-1** (2005).
12. P. H. Siegel "Terahertz Technology" IEEE Trans. Microwave Theory Tech. **50,** 910–928 (2002).
13. J. Faist, C. Gmachl, F. Capasso, C. Sirtori, D. L. Sivco, J. N. Baillargeon, and A. Y. Cho "Distributed feedback quantum cascade lasers" Appl. Phys. Lett. **70,** 2670–2672 (1997).
14. L. Mahler, R. Köhler, A. Tredicucci, F. Beltram, H. E. Beere, E. H. Linfield, D. A. Ritchie, and A. G. Davies "Single-mode operation of terahertz quantum cascade lasers with distributed feedback resonators" Appl. Phys. Lett. **84,** 5446–5448 (2004).
15. D. Hofstetter, J. Faist, M. Beck, and U. Oesterle "Surface-.emitting 10.1 μm quantum-cascade distributed feedback lasers" Appl. Phys. Lett. **75,** 3769–3771 (1999).
16. M. Plihal and A. A. Maradudin "Photonic band structure of two-dimensional systems: The triangular lattice," Phys. Rev. B **44,** 8565–8571 (1991).
17. C. Sirtori, C. Gmachl, F. Capasso, J. Faist, D. L. Sivco, A. L. Hutchinson, and A. Y. Cho "Long-wavelength ($\lambda \approx 8$ - 11.5 μm) semiconductor lasers with waveguides based on surface plasmons" *Opt. Lett.* **23,** 1366–1368 (1998).
18. G. Scalari, N. Hoyler, M. Giovannini, and J. Faist "Terahertz bound-to-continuum quantum-cascade lasers based on optical-phonon scattering extraction" Appl. Phys. Lett. **86,** 181101-3 (2005).
19. M. Meier, A. Mekis, A. Dodabalapur, A. Timko, R.E. Slusher, J. D. Joannopoulos, and O. Nalamasu "Laser Action from two-dimensional distributed feedback in photonic crystals" Appl. Phys. Lett. **74,** 7-9 (1999).
20. R. Ferrini, R. Houdré, H. Benisty, M. Qui, and J. Moosburger "Radiation losses in planar photonic crystals: two-dimensional representation of hole depth and shape by an imaginary dielectric constant" J. Opt. Soc. Am. B **20,** 469–478 (2003).
21. J. D. Joannopoulos, R. D. Meade, and J. N. Winn *Photonic Crystals: Moulding the Flow of Light* (Princeton University Press, New Jersey, 1995).

1. Introduction

Since their inception enormous progress has been made in both Quantum Cascade Lasers (QCLs) [1, 2] and Photonic Crystals (PhCs) [3, 4, 5, 6]. This is due in large part to the advances in semiconductor growth and processing technology. QCLs have steadily progressed towards low threshold, high power, room temperature operation in the Mid-Infrared (MIR) spectral range [2]. More recently, advances have been made for the far-infrared (30-300 μm, i.e. 1-10 THz) [7, 8, 9]. Likewise, PhC losses have been drastically reduced, for example at telecom wavelengths (1.55 μm) reported losses [10] are as low as 2.0 dB/cm [11] for high index contrast waveguide structures. Thus, PhCs are now becoming a viable solution for integrated optics applications.

Although extensive applications exist for Terahertz (THz) frequencies such as imaging, chemical sensing and astronomy [12], progress is needed to create versatile and bright sources, focussing not only on generation but also on compact efficient light guiding solutions. The necessary material growth thicknesses of epitaxial layers for vertical refractive index guiding at THz frequencies make them impractical. PhCs enable the control of light propagation on its wavelength scale and as such can offer versatile, small all on-chip light guiding solutions for THz QCLs. There are two aspects which particularly suit a marriage between PhCs and QCLs: Firstly, as QCLs use only one carrier type for light generation, in our case electrons, no surface recombination occurs. Secondly, as QCLs are intersubband devices the polarization selection rules require that they emit in the Transverse Magnetic (TM) direction (i.e. electric field perpendicular to the growth direction). This results in emission that is predominantly in-plane, which is well adapted to planar PhCs. Moreover, at these long wavelengthis the impact of fabrication imperfections, which still limits PhC performances [10] is reduced.

Control of emission from QCLs through gratings was introduced at MIR wavelengths as early as 1997, when Faist *et al.* [13] used Distributed Feedback lasers (DFBs) to obtain single mode operation for gas sensing applications; DFBs used to obtain single mode operation normally result in linewidths limited by the experimental set-up resolution. Recently a DFB-QCL operating at 63 μm [14] was demonstrated by etching a grating into the upper cladding, periodically changing the penetration depth of the optical mode into the metallic plasmon guiding surface and thus its effective refractive index. As QCLs emit in TM they cannot easily be configured as a vertical cavity surface emitter. However, DFBs can be used on as a second order grating to diffract the emission vertically, such that single mode vertical emission can be obtained [15].

So far little work has been done to incorporate PhCs in QCL design. In the seminal work by Colombelli *et al.* [6], a MIR (8 μm) single plasmon guided QCL structure used PhCs to enable lasing through a feedback process, i.e. propagation in a slow light mode in the transmission band of the PhC structure, and vertical extraction by acting as diffraction grating. In contrast to this work, PhCs were used by tailoring their equi-frequency surfaces in their transmission bands, here PhCs are used at their 'stopband' energies, i.e. as reflectors, and are positioned on either side of the QCL active region.

2. Design and Fabrication

To establish a suitable periodic perturbation of the dielectric is the major challenge in creating PhCs for THz-QCLs. The effect of a periodic perturbation of the dielectric on the dispersion curve of a homogeneous material are investigated by Plane Wave Expansion (PWE) calculations [16]. Fig. 1 shows the dispersion curve for TM polarised light through a (a) homogeneous material with refractive index $n = 3.9$. Fig. 1 (b) and (c) show the dispersion of PhCs consisting of a triangular lattice of pillars with $n = 3.9$ and fill factor f = 0.4. The fill factor is defined as the surface area of the PhC motif divided by the unit cell surface area. The dispersion curves in Fig. 1(b) and (c) are that of a PhC with a small ($\Delta n = 0.3$) and large ($\Delta n = 2.6$) refractive index contrast between the pillars and the surrounding medium, respectively. Comparing Fig. 1(b) to the homogeneous medium (Fig. 1(a)), we see a splitting of the degeneracy, resulting in small energy regions of high reflectivity 'stopbands' that appear at the high symmetry points and are strongly dependent on the crystallographic direction within the PhC. Increasing the refractive index contrast, as is the case in Fig. 1(c), broadens the stopbands until eventually a high reflectivity exists independent of the direction of light propagation i.e. 'full bandgap'.

The preferred method to obtain a modulation of the refractive index is by etching the pillars or holes into the dielectric structure. PhC structures for telecommunication wavelengths use planar dielectric waveguides which provide good vertical confinement of the optical mode, reducing the necessary etch depths, and facilitating the in and out light coupling with standard techniques. At THz frequencies the necessary epitaxial growth thicknesses for dielectric waveguides are impractical, single plasmonic waveguiding at the metal semiconductor interface provides a standard solution to vertical light confinement at wavelengths greater than 15 μm [17]. Single plasmon waveguide are easily fabricated and enable high power structures with little out-of-plane losses. A pictorial representation of the PhC-QCL with a single plasmon waveguide is shown in Fig. 2(a) and (b). Fig. 2(c) and (d) shows the electric field intensity versus depth into our QCL structure, calculated using the transfer matrix method. Growing a heavily doped buried layer (≈ 15 μm buried into the structure) helps to increase the confinement of the electric field in the active region, as well as serving as part of the bottom contact. The optical mode overlap with the gain region (top contact region profile in Fig. 2(c)) is Γ=0.35 [18]. A plasmon between the pillars (etch depth of 15 μm) is created by depositing a metal layer. A 5nm/50nm Ti/Au layer is deposited at this lower layer, which results in a surface plasmon, see also Fig. 3(a), this helps vertical confinement and mode matching (see Fig. 2).

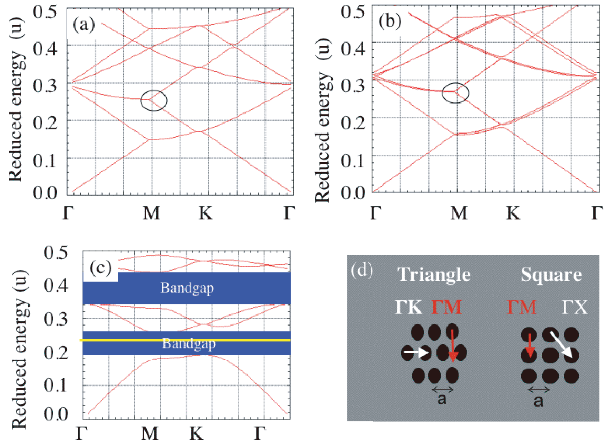

Fig. 1. 2D dispersion curves obtained from PWE calculations for TM polarised light through (a) a homogeneous medium $n = 3.9$ and, (b) and (c) a triangular PhC made of pillars, each with a refractive index difference Δn. The energy is given in reduced units u = a / λ where 'a' denotes the lattice constant and 'λ' represents wavelength. The fill factor is 0.4, the refractive index of the pillar is kept at $n = 3.9$. (b) $\Delta n = 0.3$, a weak refractive index contrast results in a splitting of the degeneracy of the high symmetry points. The circle highlights the stopband where lasing occurs in the ΓK direction. (c) $\Delta n = 2.9$ this refractive index contrast is strong enough to create full bandgaps, energy regions where the reflectivity remains high regardless of the direction of propagation in the PhC. (d) Sketch of the principal crystallographic directions in the square (triangle) lattices: ΓM and ΓX (ΓM and ΓK).

Since $\approx$ 65 % of the light is propagating in the substrate, the difference between the mode profiles in and between the pillars is such that the modulation of the effective refractive index does not considerably effect the optical mode.

As seen from Fig. 1 even a small perturbation in the refractive index will give stopbands in certain directions. Our current technology enables 4 μm pillars with an etch depth of slightly more than 15 μm, i.e. stopping at the heavily doped layer.

An important point to note is that there is a mode mismatch at the interface between the pillar and the etched regions, that can generate out-of-plane losses, see Fig. 2(c) and (d). To maintain reasonable losses and a sufficiently large bandgap a compromise fill factor of 0.4 was used in our structures [20]. However, it should be noted that out-of-plane losses are expected to be less for TM polarisation than TE [5]. Hence, the fact that QCL emission is TM naturally reduces losses in these structures when compared to predominantly TE emitting structures.

To design the optimum PhC structure PWE and 2D finite difference time domain calculations of the band diagrams and transmission spectra were used. Pillars (as opposed to holes) consistently showed larger bandgaps for TM polarisation; it is well known that isolated areas of high index material exhibit larger bandgaps for TM polarised light in contrast to TE polarised light, which favours a network of connected high index material [21].

PWE calculations for triangular and square arrays were performed for different fill factors along all the main crystallographic directions for square and triangular arrays, see Fig. 1(d). The bandgap versus fill factor for triangular arrays give larger bandgaps for our structures; in general triangular PhC arrays display larger bandgaps due to their higher symmetry.

The GaAs/$Al_{0.15}Ga_{0.85}As$ QCL structure was grown using molecular beam epitaxy on a semi-insulating GaAs substrate. It consists of 120 periods of the active regions, bounded by

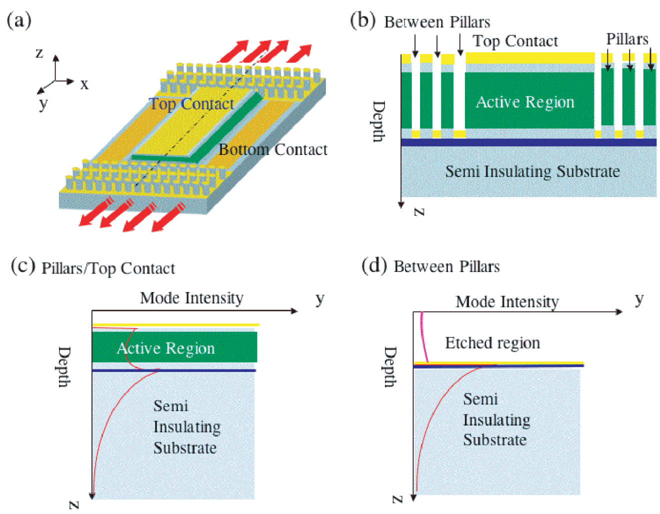

Fig. 2. (a) Schematic of QCL laser bounded by a Single Plasmon Waveguide PhC. The red arrows show the direction of the light emission. The green stripe represents the active region, the blue the heavily doped region and yellow represents metal. The top and bottom contacts are labelled. (b) Cross-section of schematic shown in (a). The electric field intensity (red line) versus vertical distance from the surface of the QCL structure for the single plasmon waveguide structure, at the pillars/top contact area (c) and between the pillars (d). The optical mode overlap with the gain region at the pillars/top contact for the the single plasmon waveguide is Γ=0.35 [18]. The mode extends over 100 μm into the QCL substrate. (d) Shows also a second mode between the top gold layer and air (violet line, not to scale) which will be coupled into by the guided mode.

two heavily doped regions which serve as contacts for the structure, see Fig. 3(a). The active region was based on the ‘bound-to-continuum’ design combined with a longitudinal optical phonon extraction mechanism as described in reference [18].

The devices were made using standard fabrication methods: The ridge waveguide is obtained by wet etching through the whole active region down to the heavily doped. The bottom contact (area 220 μm x 1 mm) is composed of an alloyed (400°C 1 min) Ni/Ge/Au/Ni/Au (10/20/50/20/200 nm) layer. The top Schottky contact area (120 μm x 1 mm) consists of a Ti/Au (3/400 nm) layer. This contact, together with a 700 nm thick heavily doped (2 x 10^{18} cm^{-3}) buried layer, forms a single plasmonic waveguide.

Due to the long wavelengths, the corresponding PhC lattice constants ‘a’ are large, $\approx$ 21 μm and a fill factor of 0.4 results in the smallest pillar radius $\approx$ 4 μm, which is well within the standard UV photolithography fabrication tolerances ($\approx$ 0.5μm). However, due to the large number of growth periods in vertical direction required for the QCL and the long emission wavelength, large etch depths are needed for the PhC to impact on the optical mode. To obtain large etch depths a mask transfer into 800 nm of SiO_2 was performed; a standard photolithographic procedure defined the pillar mask pattern in the photoresist. A CHF_3 based Reactive Ion Etch (RIE) was used to transfer the photoresist mask into the SiO_2. After removing the photoresist the pillars were etched by a Cl_2 - based RIE. Approximately two hours are needed to obtain the etch depth of 15 μm, see Fig. 3(c).

A schematic of the final structure can be seen in Fig. 3(a) along with Scanning Electron Microscope (SEM) pictures of the top (Fig. 3(b)) and side (Fig. 3(c)) of the structures. Very

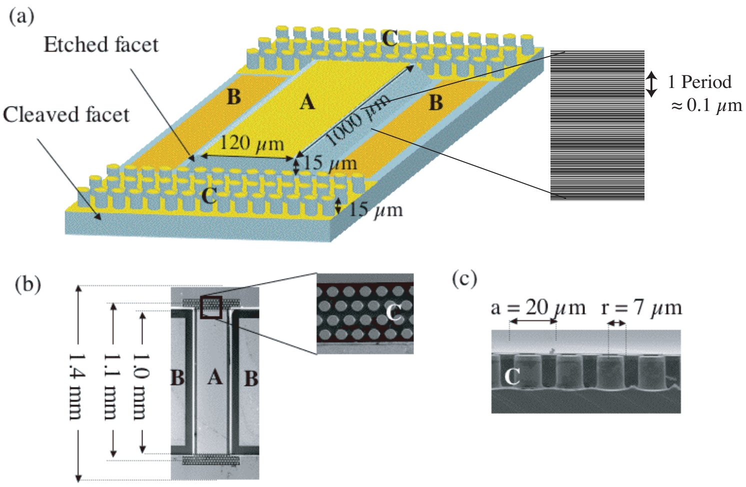

Fig. 3. Schematic and Scanning Electron Microscope (SEM) images of a fabricated structure. (a) Schematic shows the top '**A**' and bottom '**B**' contacts and the ridge waveguide (below the top contact) bounded by four rows of PhC pillars '**C**' on either side. (b) SEM image shows a top view of a ΓM orientated PhC-QCL, with a corresponding enlargement of the PhC area. (c) SEM image shows the cross section taken through the pillar structure after metal deposition. Good vertical sidewalls over the entire 15 μm depth are shown.

good side wall verticality was obtained for the entire 15 μm depth.

3. Experimental Results

The first test structure consists of a QCL bounded by 4 rows of a ΓK oriented triangular lattice PhC, i.e. light propagates in the ΓK direction of the PhC, with a period of 21 μm. Lasing action is observed under both continuous wave and pulsed (duty cycle of 0.008 %) excitation at 9 K. The current voltage and output light versus injected current curves for a structure under pulsed excitation are presented in Fig. 4(a). The output light peak power was measured by collecting the laser emission using a light pipe and sending it to a broadband, calibrated thermopile. The performance of the laser is good: a lasing threshold of J_{th} = 421 A/cm^2 and a peak optical output power of 2 mW were measured.

The current light curve shows a linear increase of the output power up to a current density of 750 A/cm^2. As shown in Fig. 4(a) lasing action was observed up to liquid nitrogen temperatures (77 K) in pulsed mode.

High resolution (0.03 meV) spectra were taken using a Fourier Transform Infra-Red (FTIR) spectrometer with a cryogenically cooled bolometer lock-in detection system. Fig. 4(b) shows the spectrum taken at 9K at four different currents each marked with a symbol on Fig. 4(a). These spectra display singlemode emission at λ = 81.7 μm until roll over unlike their Fabry-Pérot counterparts that show blue shift of the order of the mode envelope due to a Stark shift of the lasing transition [18]. Hence, a stable singlemode emission is shown for the whole dynamic range of the PhC-QCL device.

Lasing action is observed at u = 0.26 in reduced energy units, that corresponds exactly to the

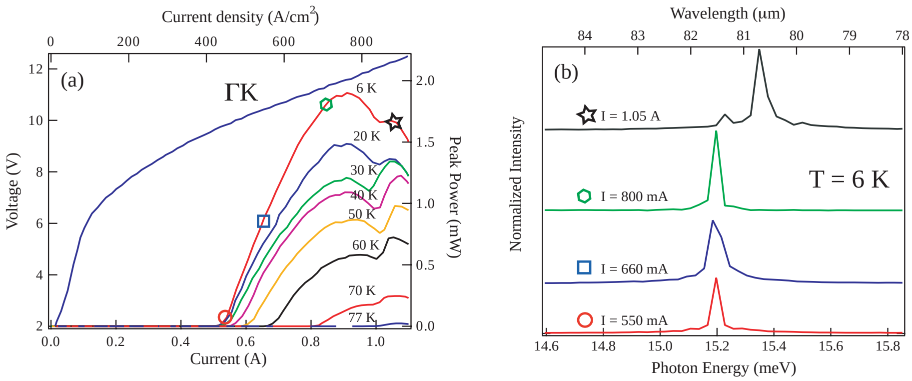

Fig. 4. Results from a 4 row PhC-QCL in the ΓK directions a = 21 μm (a) Current voltage and output light peak power was measured by collecting the laser emission using a light pipe and sending it to a broadband, calibrated thermopile, and a series of light current curves for increasing temperatures. Lasing action upto liquid nitrogen temperatures is observed (temperature range 6 - 77 K). versus injected current with a current threshold, J_{th}, = 421 A/cm^2. (b) Series of high resolution spectra taken at different currents. Each current is marked on Fig. 4(a) with the corresponding symbol. The emission starts single mode at the lasing threshold and remains single mode with increasing current, moreover no wavelength drift with increased current is observed, until lasing roll over.

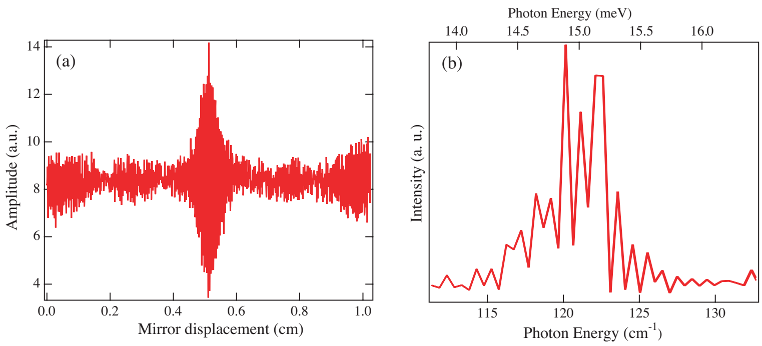

Fig. 5. Results from a 4 row PhC-QCL in the ΓK directions with a = 21 μm. Sub threshold (a) Interferogram showing beating and (b) Optical spectrum, the spacing of the Fabry-Pérot fringes corresponding to an optical path length of 1.1 mm.

degeneracy point at ΓK point, shown within the circle on Fig. 1(a) and (b); [1] i.e. the solution of the first order Bragg condition. There is a high reflectivity at this point as the degeneracy is broken by a small periodic perturbation, such as that introduced by our planar PhCs. The narrow stopband has a higher reflectivity than the cleaved or etched facets as is attested to by the lasing action that occurs from reflections at the PhC. Since the reflectivity is high within a narrow energy band along the ΓK direction singlemode emission with no wavelength drift is observed even when the gain curve shifts. In fact, as long as the width of the high reflectivity stop band is smaller than the free spectral range of the optical cavity the emission will remain singlemode.

[1] Note that the point appears to be located at the ΓM point in Fig. 1(a) and (b) due to a peculiarity of band folding in the reduced brillouin zone scheme where ΓM fold onto ΓM, but ΓK, folds on to ΓK,ΓM,ΓK

Several tests were performed to ensure lasing resulted from reflections at the PhCs, and not from reflections of either the cleaved facet or the etched facet of the ridge waveguide, One confirmation is given by the fact that the sub-threshold Fabry-Pérot fringe spacings, seen as beating in the interferogram of Fig. 5(a) and as fringes spacing in Fig. 5(b), corresponds to the correct optical path distance of 1.1 mm (see Fig. 3(b)) when assuming an effective index for the guided mode of n_{vg} = 3.9 [18]. Having a 1 mm long ridge waveguide (see Fig. 3) implies that the region of high reflectivity is inside the pillar structure. Moreover, the spacing of the sub-threshold Fabry-Pérot fringes of a sample cleaved just after the pillars on one side of the laser but 2.5 mm from the ridge waveguide on the other side of the laser were analysed. The fringes continue to correspond to an optical path length of 1.1 mm. This definitively precludes lasing due to reflections at the cleaved facets. To further rule out the possibility that lasing could be attributed to reflections at the etched facets of the ridge waveguide, a device was fabricated without pillars, i.e. a ridge waveguide bounded by a plateau etched to a depth of where the pillars were in the previous structure. In this case the sub-threshold Fabry-Pérot fringe spacings correspond to an optical path length of that of the cleaved facets (i.e. 1.4 mm), see Fig. 3(b). Thus, we conclude that the lasing action does not occur from reflections at either the cleaved facet, nor the etched facet, but at the pillars.

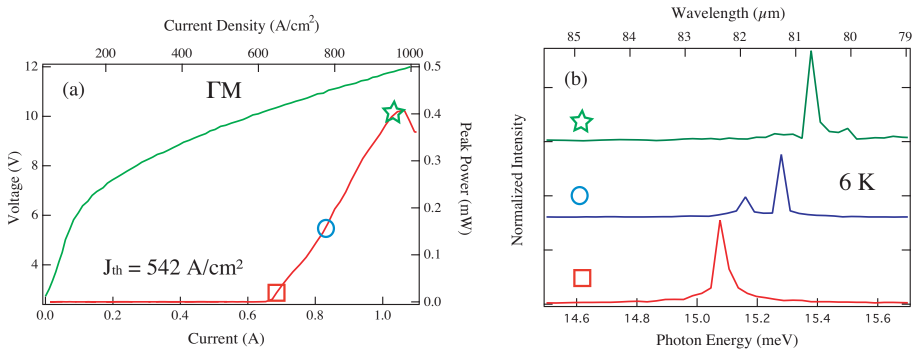

Fig. 6. Results on a 4 row PhC-QCL in the ΓM directions with a = 21 μm (a) Current voltage and output light versus injected current showing a J_{th} = 542 A/cm^2. (b) Series of high resolution spectrum taken at different currents showing multi mode emission, a blue shift with increased current is seen due to the quantum confined Stark effect.

The second structure measured is the twin of the first structure, except that the PhC is aligned in the ΓM direction. Fig. 6(a) shows the current versus voltage and the output light versus injected current curves. The structure exhibits a 24 % higher threshold, J_{th} = 546 A/cm^2, than that measured in the ΓK device. The high optical saturation which occurs at 875 A/cm^2 can be explained by the fact that the cavity is broadband and the peak gain can be exploited. The threshold currents and saturation densities of the structures are typical for Fabry-Pérot THz-QCLs [18]. When compared to the ΓK device, not only is the threshold higher, but more striking is the contrasting behaviour of the spectra, see Fig. 6(b). Here, the emission is clearly multimode, and shows a Stark blue shift of the lasing peak with increasing current. The lasing wavelength just above threshold is 82.2 μm and shifts to 79.7 μm just before roll over[2]. Hence, the small periodic dielectric perturbation introduced by our 2D-PhC has a negligible effect on the reflectivity seen by the lasing wavelength. These results concur with the fact that there is a higher threshold

[2]The spacing between the modes can be seen clearly on the spectra taken at 0.8 A (blue line Fig. 5(b)). The optical path calculated from the sub-threshold Fabry-Pérot fringes using an n_{gr} = 3.9 is 1.3 mm that suggests that the highest reflectivity is at the cleaved facets.

obtained from the ΓM than the ΓK orientated PhCs. The lasing behaviour in the ΓM orientated PhC structure suggests a flat low broadband reflectivity, thus unsurprisingly when the peak of the gain curves shift, the mode hops to the next lasing mode. The free spectral range between these lasing modes, corresponding to an optical path of 1.3 mm, suggest that lasing occurs due to reflection at the cleaved facets.

4. Conclusion

To conclude, we have designed and fabricated electrically injected all on chip THz PhC-QCLs. Two different symmetry directions of the PhC triangular lattice were tested, ΓM and ΓK. Dramatically different results were obtained: For light propagating in the ΓK direction singlemode emission with no wavelength drift with increasing current was observed whilst for light propagation in the ΓM direction multimode emission was blue shifted with increasing current. These results were explained by the high reflectivity points in the dispersion curve of the PhC. Further work is being carried out to increase the PhC effect by means of a metal-metal confinement between the pillars.

We would like thank to the Swiss National Center of Competence in Research (NCCR) for providing funding through the Quantum Photonics project.